Effect of chemical pressure induced by La^{3+}/Y^{3+} substitution on the magnetic ordering of $(AMn_3)Mn_4O_{12}$ quadruple perovskites

M. Verseils,[1] F. Mezzadri,[2] D. Delmonte,[2] B. Baptiste,[1] Y. Klein,[1] S. Shcheka,[3] L. C. Chapon,[4,*] T. Hansen,[4] E. Gilioli,[2] and A. Gauzzi[1]

[1]*Institut de Minéralogie, de Physique des Matériaux et de Cosmochimie - Sorbonne Université, UPMC, CNRS, IRD, MNHN 4, place Jussieu, 75005 Paris, France*

[2]*Istituto dei Materiali per Elettronica e Magnetismo, CNR, Area delle Scienze, 43100 Parma, Italy*

[3]*Bayerisches Geoinstitut, University of Bayreuth, 95440 Bayreuth, Germany*

[4]*Institut Laue-Langevin, 71 avenue des Martyrs, 38000 Grenoble, France*

(Received 20 June 2017; published 28 November 2017)

We report on the successful high-pressure synthesis of single-phase powders of the quadruple perovskite $(YMn_3)Mn_4O_{12}$, where the chemical pressure exerted by the small Y^{3+} ion is expected to enhance the exchange interaction between Mn^{3+} ions. According to this expectation, powder neutron diffraction, specific heat, and magnetization measurements give evidence of a C-type antiferromagnetic ordering of the Mn^{3+} ions in the octahedrally coordinated B sites at $T_{N,B} = 108$ K, 30 K higher than in the isostructural and isovalent compound, $(LaMn_3)Mn_4O_{12}$. Surprisingly, we found no evidence of long-range magnetic order of the square-coordinated A' sites, although an indication of latent magnetic order is given by a broad peak of the DC magnetization between 70 and 40 K and by a sharp peak in the AC susceptibility at $T^* = 70$ K. A further unexpected feature of $(YMn_3)Mn_4O_{12}$, not found in previously reported $(AMn_3)Mn_4O_{12}$ compounds, is a second-order structural phase transition at $T_s = 200$ K, attributed to a partial redistribution of charge involving both the B and A'-site Mn^{3+} ions. The present results suggest the existence of competing magnetic orderings, which may be linked to the occurrence of magnetic ferroelectricity in the $(AMn_3)Mn_4O_{12}$ system.

DOI: 10.1103/PhysRevMaterials.1.064407

I. INTRODUCTION

Quadruple perovskites, described by the general formula $(AA'_3)B_4O_{12}$, have recently attracted a great deal of interest for they display unique charge, spin, and orbital orderings not found in simple perovskites, ABO_3. These properties arise from a unique pseudocubic structure shown in Fig. 1, first reported by Marezio *et al.* [1], which hosts two distinct A and A' sites. The structure is stabilized by the Jahn-Teller distortion of the latter sites, typically occupied by Cu^{2+}, as in the prototype compound $CaCu_3Ti_4O_{12}$ reported by Deschanvres *et al.* [2], or by Mn^{3+}, as in the present case. The distortion turns the pristine dodecahedral coordination of the A' sites into square planar and drives a very large tilt of the corner-sharing BO_6 octahedra, the tilt angle $\psi \sim 137^\circ$ being much larger than that found in simple perovskites. The resulting structure is characterized by two distinct B-O-B and A'-O-B zigzag superexchange paths with competing antiferromagnetic (AFM) or ferromagnetic (FM) interactions, which accounts for the variety of ground states observed. The square coordination of the A' sites also accounts for the absence of oxygen defects in quadruple perovskites, as these defects would destabilize the bond structure. This feature constitutes a further important difference as compared to simple perovskites where oxygen nonstoichiometry greatly affects the physical properties. In the present paper, we consider the quadruple perovskite $(AMn_3)Mn_4O_{12}$ family where both A' and B sites are occupied by Mn. Among the remarkable properties observed in these compounds, notable are the full charge order in the mixed-valence compound $(NaMn_3)Mn_4O_{12}$ [3] and the large values of electric polarization induced by magnetism in $(CaMn_3)Mn_4O_{12}$ [4], attributed to a peculiar helicoidal orbital and magnetic order [5,6].

The above orderings remain poorly understood because of a complex interplay between charge, spin, and orbital degrees of freedom, which makes the development of realistic theoretical models challenging. In the absence of reliable models, in the present paper we investigate the effect of chemical pressure on the stability of the magnetic structure, as the exchange interaction is sensitive to bond angles and bond distances of the superexchange paths. We consider the comparatively simple case of single valent Mn^{3+} systems where only the spin and orbital degrees of freedom come into play. Specifically, we report on the successful high pressure synthesis of high-purity $(YMn_3)Mn_4O_{12}$ powders, where the Y^{3+} ion ($R_{Y^{3+}} = 1.1$ Å [7]) is significantly smaller than all the A ions (La^{3+}, Bi^{3+}, Ca^{2+}, Na^+, Pr^{3+}, Pb^{2+}) previously reported for the $(AMn_3)Mn_4O_{12}$ system [8–10]. According to our expectation, we achieved a significant increase of the ordering temperature of the B sites as compared to its isovalent counterpart with $A = La$ [11]. On the other hand, we surprisingly find no long-range magnetic order of the A' sites, which has always been observed in all $(AMn_3)Mn_4O_{12}$ compounds previously reported. Instead, at high temperature, we observe a second-order structural phase transition never observed in any of these compounds. These unexpected features suggest the existence of latent structural and magnetic instabilities in the $(AMn_3)Mn_4O_{12}$ system.

The paper is organized as follows: In Sec. II, we report on the experimental techniques employed for the synthesis and characterization of both single crystals and powder samples of $(YMn_3)Mn_4O_{12}$. In Sec. III, we present and discuss the

*Present address: Diamond Light Source, Didcot OX11 0DE, Oxon, United Kingdom.

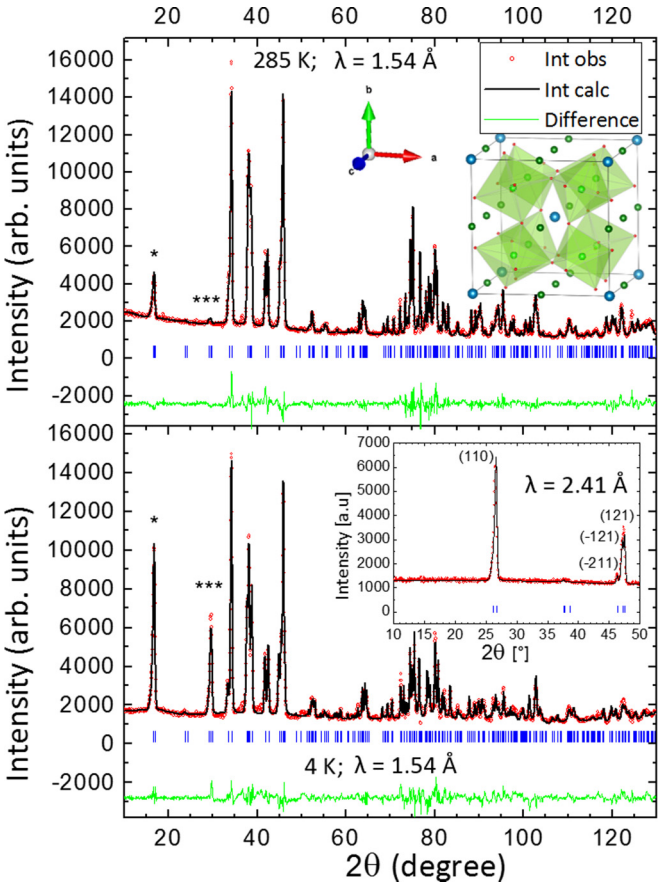

FIG. 1. Red circles: experimental neutron diffraction patterns taken at 285 K (top panel) and 4 K (bottom panel) on the $(YMn_3)Mn_4O_{12}$ powder sample using a wavelength $\lambda_1 = 1.54$ Å. Black line: calculated intensity obtained by refining the λ_1 and λ_2 patterns, as described in the text. Green line: difference between observed and calculated patterns. Inset: main magnetic peaks at 4 K measured using a neutron wavelength of $\lambda_2 = 2.41$ Å.

properties of the nuclear and magnetic structure and the result of the magnetic and thermodynamic measurements. In particular, we discuss the results with emphasis on the unexpected absence of long-range order in the A' sites. In Sec. IV, we draw the conclusions.

II. EXPERIMENTAL

A. High-pressure synthesis

$(YMn_3)Mn_4O_{12}$ single crystals and powder samples were obtained from the solid state reaction of stochiometric mixtures of Y_2O_3 and Mn_2O_3 powders filling a Pt capsule at 9 GPa and 1300 °C for two hours using a multianvil press, as described in detail elsewhere [12]. A 1000 tons multianvil press installed in the IMEM-CNR laboratory was used to optimize the synthesis conditions. A larger 6000 tons press installed at the Bayerisches Geoinstitut in Bayreuth was used to prepare a larger (∼1 g) amount of powders required for the powder neutron diffraction study. After the heat treatment, the samples were quenched to room temperature and the pressure was slowly released. Attempts to obtain the desired phase at lower pressure or at lower temperatures were not successful. A room temperature powder x-ray diffraction (xrd) analysis in the Bragg-Brentano geometry by means of a laboratory diffractometer equipped with a Cu K_α source was performed to check the purity of the as-prepared powders after each run.

B. Single-crystal x-ray diffraction

Single-crystal x-ray diffraction data were collected on an Oxford diffraction Xcalibur-S diffractometer equipped with a Sapphire CCD-detector with Mo-Kα radiation ($\lambda =$ 0.71073 Å, graphite monochromator) at 293 K. Data reduction, cell refinement, space-group determination, scaling, and multiscan absorption correction [13] were performed using *CrysaAlisPro* software [14]. The structure was solved through Olex2 program [15] by direct methods using *SHELXT* [16]. The refinement was then carried out with *SHELXL-2013* [16] by full-matrix least squares minimization and difference Fourier methods. All atoms were refined with anisotropic displacement parameters.

C. Neutrons powder diffraction

In order to systematically study the nuclear and magnetic structures as a function of temperature, a neutron powder diffraction experiment was subsequently performed on a 920 mg powder sample at the high-intensity two-axis D20 diffractometer of the Institut Laue Langevin in Grenoble (France) using $\lambda_1 = 1.54$ Å and 2.41 Å wavelengths and a 90° takeoff setup. The data were taken as a function of temperature by warming up the sample from 4 K up to room temperature at a rate of 0.25 K/min. The two wavelengths are optimized for an accurate determination of the nuclear and magnetic structures, respectively. We employed the Fullprof package [17] in the sequential and multipattern mode to perform, for each temperature, a Rietveld refinement of the nuclear and magnetic structures using the two λ_1 and λ_2 patterns with the same weight. Thermal displacement parameters were refined with anisotropic model for A' sites because of their anisotropic environment and with an isotropic model for all the other atoms.

D. Thermodynamic and magnetic properties

Constant-pressure specific heat (C_p) measurements as a function of temperature in the 2–400 K range were carried out on the same powders as above using a 2τ-relaxation method in a commercial Quantum Design™ physical property measurement system (PPMS). DC magnetization (M_{DC}) measurements were carried out in a commercial Quantum Design™ superconducting quantum interference device magnetometer (SQUID) as a function of temperature and field. A first zero-field-cooling (0-ZFC) measurement was performed after having completely removed the residual field by warming the superconducting magnet above its critical temperature. A further series of ZFC and field-cooling (FC) magnetization curves in the 10–100 Oe range were taken by minimizing the residual field before each ZFC measurement. This was accomplished by discharging the magnet in the oscillating mode. We verified that this procedure typically reduces the residual field below 0.02 Oe, as measured by means of a gaussmeter.

TABLE I. $I2/m$ crystal structure of $(YMn_3)Mn_4O_{12}$ obtained from the refinement of powder neutron diffraction data, as described in the text. The structure is given for 285 K (above T_S), 190 K (above $T_{N,B}$), and 4 K (below $T_{N,B}$). Numbers in parentheses indicate statistical uncertainty.

Temperature	**285 K**	**190 K**	**4 K**
a,b,c(Å)	7.45005(16),7.34182(14), 7.45002(16)	7.44950(17),7.32773(15), 7.45549(17)	7.47151(20),7.30317(18), 7.46605(21)
β(°),V(Å)^3	91.1214(13), 407.415(15)	91.1546(14), 406.897(16)	91.4225(16), 407.265(19)
		Y 2*a* (0,0,0)	
*B*iso	2.12(13)	1.89(13)	4.63(30)
		Mn A' 2*b* (0,1/2,0) 2*c* (1/2,0,0) 2*d* (1/2,1/2,0)	
β_{11}, β_{22}, β_{33}	0.0056(18), 0.0064(11), 0.0035(17)	0.0045(18), 0.0050(10), 0.0023(17)	0.0086(24), 0.0051(14), 0.0068(22)
β_{12}, β_{13}, β_{23}	0.0, −0.00312(78), 0.0)	0.0, −0.00339(80), 0.0	0.0, −0.0112(14), 0.0
		Mn B 4*e* (1/4,1/4,1/4) 4*f* (1/4,1/4,3/4)	
*B*iso	0.418(75)	0.368(79)	0.715(98)
		O1 4*i*(*x*,0,*z*)	
x,*z*	0.16367(85), 0.29432(79)	0.16354(80), 0.29504(82)	0.16314(83), 0.29389(89)
*B*iso O1	0.942(77)	0.808(79)	0.053(67)
		O2 4*i*(*x*,0,*z*)	
x,*z*	0.17962(88), 0.68360(87)	0.17841(92), 0.68490((91)	0.17582(94), 0.69043(99)
*B*iso O2	0.942(77)	0.808(79)	0.053(67)
		O3 8*j*(*x*,*y*,*z*)	
x,*y*,*z*	0.01260(78), 0.30824(68), 0.17224(64)	0.01311(71), 0.30816(72), 0.17168(67)	0.01341(93), 0.31512(108), 0.16776(95)
*B*iso O3	1.368(50)	1.363(54)	2.421(87)
		O4 8*j*(*x*,*y*,*z*)	
x,*y*,*z*	0.30977(65),0.17796(69), −0.00977(64)	0.30977(69),0.17867(72), −0.00928(68)	0.31427(95),0.18654(111), −0.00665(97)
*B*iso O4	1.289(57)	1.363(54)	2.421(87)
R-Bragg(λ1,λ2),Global χ^2	6.66, 6.24, 5.65	6.99, 6.60, 6.12	8.77, 5.99, 7.99
Magnetic R-factor			4.97

III. RESULTS

A. Structural properties

1. Crystal structure

The single-crystal x-ray diffraction study indicates that, at room temperature, the system crystallizes in the monoclinic $I2/m$ space group, see Supplemental Material [18] for tables refinement. This indicates that the isovalent La/Y substitution does not alter significantly the structure of the pristine $(LaMn_3)Mn_4O_{12}$ compound, as expected, which is confirmed by a subsequent powder neutron diffraction study (see Fig. 1). This study also shows that the purity of the powder sample is 95% or better. The diffractogram shows minor diffraction peaks attributed to an unknown impurity phase formed at 9 GPa. In the following, we shall limit ourselves to analyze the neutron data as a function of temperature. In the whole 4–285 K range investigated, no indication of symmetry change was detected within the experimental resolution and all patterns were successfully refined in the $I2/m$ symmetry. In the refinement, all B thermal parameters were supposed to be isotropic except those of the Mn A' sites for which the square coordination is expected to be anisotropic. For all temperatures, we obtained good refinements, such as those shown in Fig. 1, where the experimental and calculated patterns are compared for two representative temperatures, 285 K and 4 K. The quality of the refinement did not change appreciably in the whole temperature range studied. However, we noticed an anomalous increase of the B parameter of Y below $T_s = 200$ K. This indicates that the structural transition at T_s may be associated with a shift of Y ions from the centrosymmetric (0,0,0) position. The inherent limitation of the present refinement of powder diffraction data does not permit to unambiguously identify any symmetry change. A further high-resolution single-crystal study, e.g., by synchrotron x-ray diffraction, may elucidate this point.

In Table I, we report the results of the refinements of the 285, 190, and 4 K structures. As expected, the smaller Y^{3+} ion leads to a 2% smaller unit cell, $V = 407.42(2)$ Å, as compared to the isostructural compound $(LaMn_3)Mn_4O_{12}$. The room-temperature unit-cell parameters are $a = 7.4500(2)$ Å, $b = 7.3418(2)$ Å, $c = 7.4500(2)$ Å, and $\beta = 91.121(1)°$. The evolution of the structure with temperature is shown in Fig. 2. At high temperature, above T_S, the c axis and the monoclinic angle β display an unusual increase upon decreasing T. Below T_S, the a-axis parameter also increases, hence the unit-cell volume suddenly increases. This feature gives evidence for a second-order phase transition at T_s with no apparent change of space group. The neutron diffraction patterns display neither extra Bragg peaks nor changes of intensity in any peak, which indicates that the transition at T_s is nonmagnetic. A similar V-

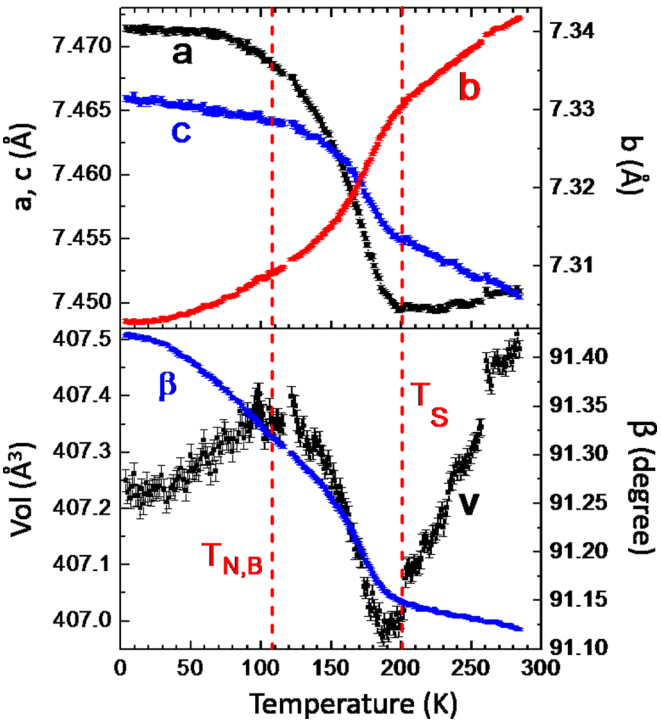

FIG. 2. Unit cell parameters and unit cell volume of $(YMn_3)Mn_4O_{12}$ as a function of temperature obtained from the refinement of the powder neutron diffraction data. Broken lines indicate the temperatures of the second order structural phase transition at T_s and of the antiferromagnetic ordering of the B sites at $T_{N,B}$.

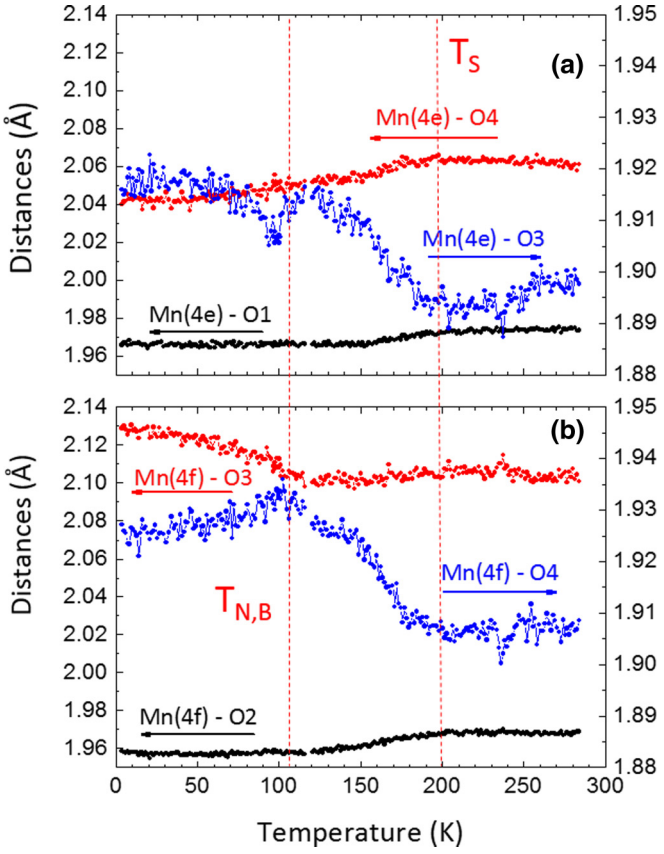

FIG. 3. Temperature dependence of the Mn-O bond lengths of the B sites obtained from the structural refinement of the powder neutron diffraction data. (a): Mn (4e) sites. (b): Mn (4f) sites. Red broken lines indicate the transitions at T_s and at $T_{N,B}$.

shaped behavior of the unit-cell volume was recently reported in $(CaMn_3)Mn_4O_{12}$ [19] where the anomaly is concomitant to a cubic-to-rhombohedral structural transition. At lower temperature, i.e., below $T_{N,B} = 108$ K, V turns back into a conventional regime with positive thermal expansion. As discussed below, this temperature corresponds to the magnetic ordering of B sites. In this temperature, no anomaly is observed in the behavior of the unit-cell parameters; all of them display a smooth temperature dependence and the cusplike behavior of V at $T_{N,B}$ is less pronounced than that at T_s. This behavior is due to a leveling off of the a-axis dependence and to a smaller expansion rate of the c-axis parameter, while b continues to decrease rapidly.

In order to gain an insight into the origin of the transitions at T_s and at $T_{N,B}$, we analyze the temperature dependence of the relevant Mn-O bond-length distances for the A' ($2b$, $2c$, $2d$) and B sites ($4e$, $4f$), as shown in Figs. 4 and 3, respectively. Representative values of these distances and of the corresponding Jahn-Teller (JT) distortion parameters, Δ_{JT}, for the B sites are reported in Table II. The Δ_{JT} values for the two octahedra are slightly different and somehow larger than in $(CaMn_3)Mn_4O_{12}$ [20] but smaller than in $(LaMn_3)Mn_4O_{12}$ [11]. At both transition temperatures, T_s and $T_{N,B}$, almost all distances exhibit more or less pronounced discontinuities in the slope. Namely, the bond lengths having a dominant component along the b axis, e.g., Mn($2c$)-O4, Mn($2b$)-O3, Mn($2d$)-O4, Mn($4e$)-O1, and Mn($4f$)-O2 (see Table II) display a conventional behavior in the T_s–$T_{N,B}$ range. On the other hand, the bond lengths mainly contained in the ac plane, e.g., Mn($4e$)-O3, Mn($4f$)-O4, Mn($2d$)-O2, Mn($2d$)-O1, Mn($2b$)-O1, and Mn($2b$)-O2, exhibit an anomalous increase with decreasing temperature. This difference is consistent with the change in the unit cell parameters discussed above and suggests a magnetostriction below $T_{N,B}$ which mainly involves the two shortest A'-O bonds, Mn($2b$)-O3 and Mn($2c$)-O4. In order to further analyze the structural changes occurring at T_s and at $T_{N,B}$, we calculated the bond valence sum (BVS) for all B and A' sites. For the latter sites, we included the four next-nearest oxygen neighbors to obtain a realistic estimate of the valence. The result of the analysis is reported in Fig. 5. At first sight, the changes observed at T_s and $T_{N,B}$ are explained by a small charge redistribution, as observed in other quadruple perovskites [21] or by a change in the orbital occupancy. However, since the changes are much more pronounced at $T_{N,B}$, the changes may simply reflect a variation of internal strain, consistent with a scenario of magnetostriction, as discussed by Goodenough in the case of doped manganites with simple perovskite structure [22].

2. *Magnetic structure*

In Fig. 1, the temperature dependence of the diffraction patterns reveals an increase of the intensity of the (110), (−211), (−121), and (121) peaks at $T_{N,B}$, which indicates a

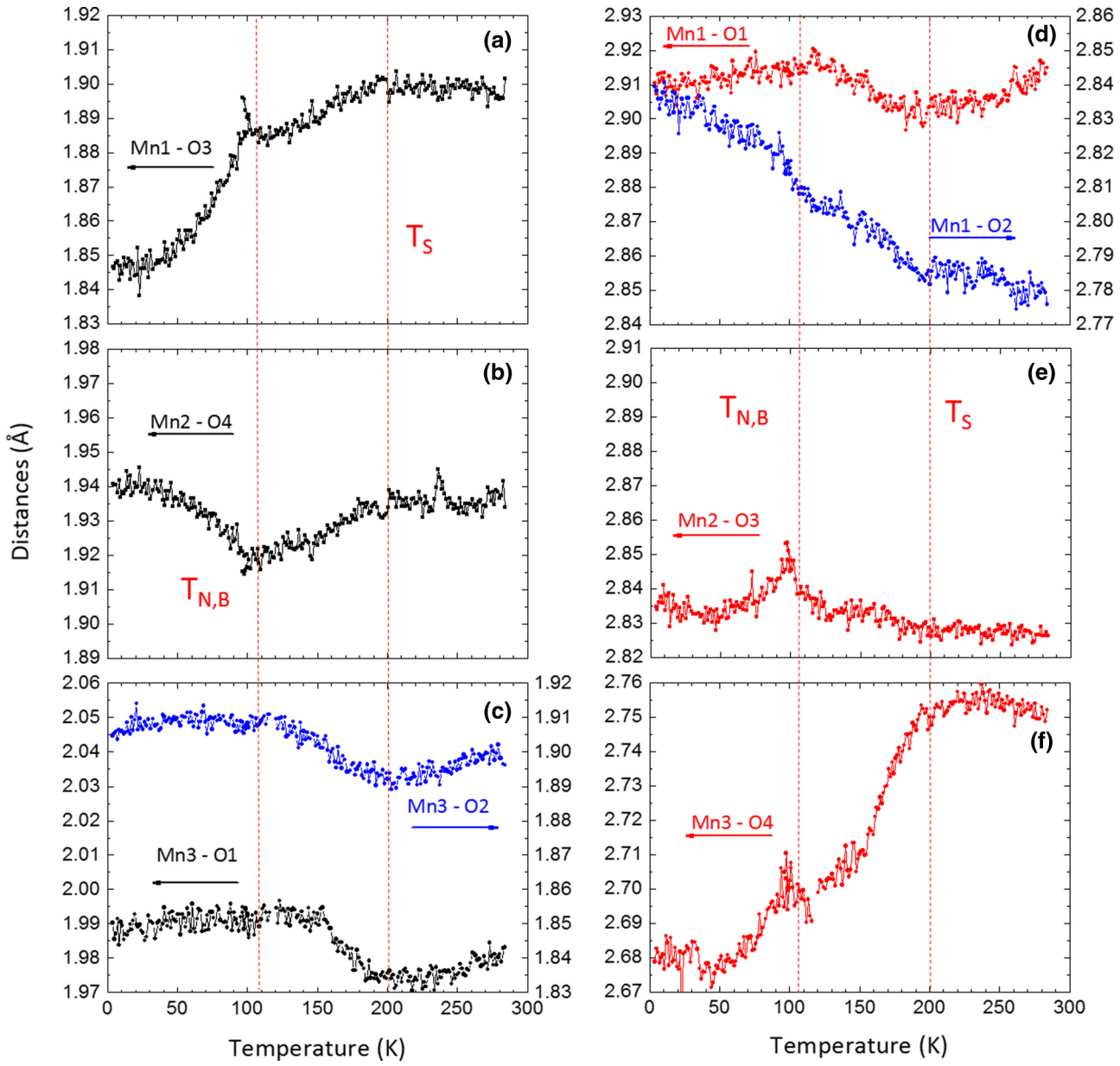

FIG. 4. Mn-O bond lengths of the A' sites as a function of temperature. Left panels: Mn-O bond lengths of the square-planar coordinated Mn(2b), Mn(2c), and Mn(2d) A' sites. Right panels: the same as before for the Mn(2b), Mn(2c), and Mn(2d) A' sites. Red broken lines are as above.

long-range magnetic ordering with $\mathbf{k} = (0,0,0)$ propagation vector. A straightforward symmetry analysis indicates two distinct irreducible representations (irrep) corresponding to the $I2'/m'$ and $I2/m$ magnetic groups describing the magnetic structure. For each one of these two irreps, we have considered the three possibilities of ordering of the A' sites alone, of the B sites alone and of both sites. We obtained a successful refinement of the data only for the $I2'/m'$ structural model where the B sites are ordered while the A' sites are not. No refinement including the ordering of the A' sites converged. The absence of magnetic order of the A' sites in $(YMn_3)Mn_4O_{12}$ is surprising as the opposite result was reported for all previous $(AMn_3)Mn_4O_{12}$ compounds [3,9,11].

By taking into account the cubic pseudosymmetry of the $I2/m$ crystal symmetry, we shall finally propose the magnetic structure reported in Table III and shown in Fig. 6 where the magnitude of the magnetic moment is the same for the two 4e and 4f B sites. This is a C-type structure similar to that previously reported for $(LaMn_3)Mn_4O_{12}$, where the coupling is AFM within the ac plane and FM along the b axis. The good quality of the refinement is apparent from the inset of Fig. 1 and from Table III, where we report the refined structure for the lowest temperature measured, 3.7 K. At this temperature the refined value of the magnetic moment is $\mu = 3.5(7)\ \mu_B$/Mn, somehow lower than the value of 4.0 μ_B expected for the Mn^{3+} ion in the high spin state ($S = 2$). It is well known that this reduction reflects the semicovalent character of the Mn-O bond in manganites. Notable is the pronounced canting of the moments along the b axis explained by a Dzyaloshinskii-Moriya (DM) interaction [23] expected in

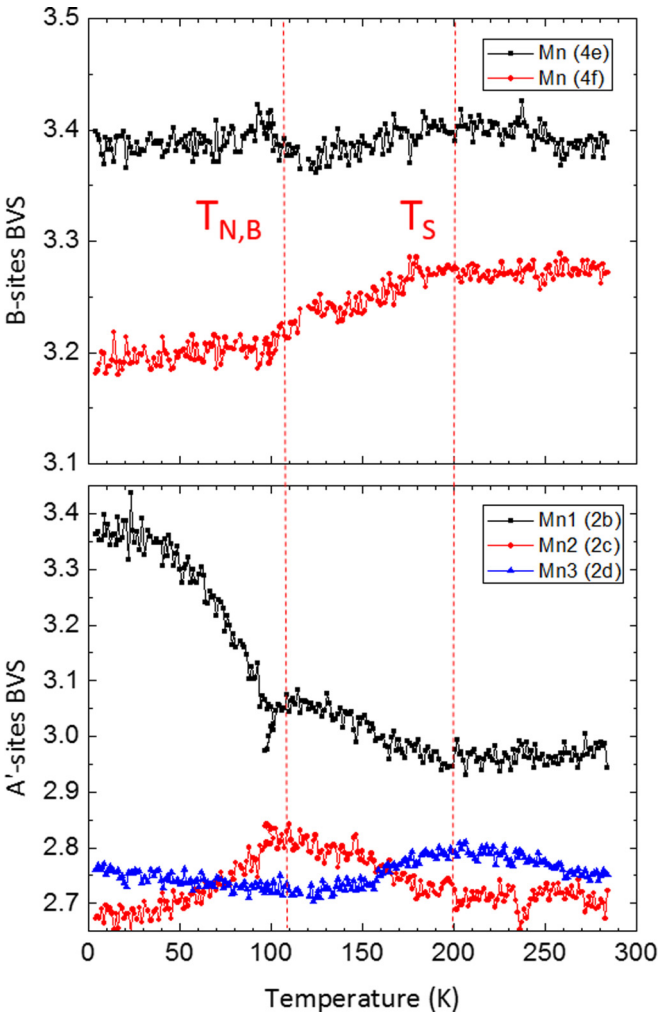

FIG. 5. Temperature dependence of the bond valence sum (BVS) of the Mn sites of $(YMn_3)Mn_4O_{12}$. Upper panel: B sites ($4e$ and $4f$). Lower-panel: A' sites ($2b$, $2c$, and $2d$). Red broken lines are as above.

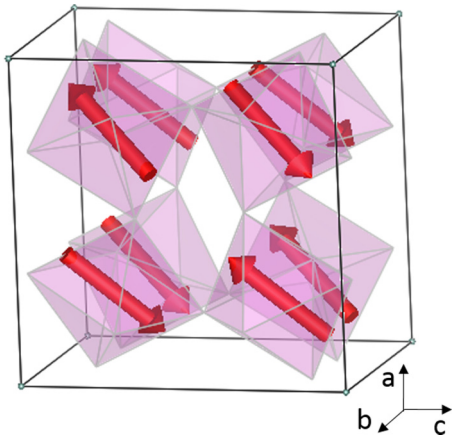

FIG. 6. C-type magnetic structure of $(YMn_3)Mn_4O_{12}$ as determined from the refinement of the neutron data (see Table III). Note the pronounced canting of the moments along the b axis, as described in the text.

TABLE II. Mn-O bond lengths (in Å) for the Mn A' and B sites at the representative temperatures of 284, 190, and 4 K obtained from the data of Table I. Numbers in parentheses indicate statistical uncertainty. $\Delta_{JT} = \frac{1}{3}\sum_{i=1}^{3}[\frac{(d_i-\bar{d})}{\bar{d}}]^2$ indicates the Jahn-Teller parameter, where i labels the three inequivalent bonds of the MnO_6 octahedron.

Temperature	Bond orientation	285 K	190 K	4 K
***A′* sites**				
Mn(2*b*)-O1 (×2)	*ac* plane	2.915(7)	2.908(7)	2.910(7)
Mn(2*b*)-O2 (×2)	*ac* plane	2.776(8)	2.786(8)	2.839(8)
Mn(2*b*)-O3 (×4)	*bc* plane	1.902(8)	1.898(8)	1.847(8)
Mn(2*c*)-O3 (×4)	*bc* plane	2.826(8)	2.829(8)	2.835(8)
Mn(2*c*)-O4 (×4)	*ab* plane	1.934(8)	1.935(8)	1.941(8)
Mn(2*d*)-O1 (×2)	*ac* plane	1.983(7)	1.974(7)	1.990(7)
Mn(2*d*)-O2 (×2)	*ac* plane	1.896(8)	1.897(8)	1.905(8)
Mn(2*d*)-O4 (×4)	*bc* plane	2.752(8)	2.746(8)	2.679(8)
B sites				
Mn(4*e*)-O1 (×2)	∼*b* axis	1.973(3)	1.973(3)	1.966(3)
Mn(4*e*)-O3 (×2)	∼*a* axis	1.898(7)	1.895(7)	1.916(7)
Mn(4*e*)-O4 (×2)	∼*c* axis	2.061(7)	2.060(7)	2.040(7)
$\Delta_{JT}(4e)$		0.00114	0.00117	0.00066
Mn(4*f*)-O2 (×2)	∼*b* axis	1.969(3)	1.966(3)	1.958(3)
Mn(4*f*)-O3 (×2)	∼*a* axis	2.101(7)	2.106(7)	2.129(7)
Mn(4*f*)-O4 (×2)	∼*c* axis	1.909(7)	1.909(7)	1.927(7)
$\Delta_{JT}(4f)$		0.00162	0.00171	0.00195

tilted perovskitelike structures. In the present case, the canting angle of the moment with respect to the *ac* plane is as large as ∼20°, much larger than previously reported in the counterpart simple-perovskite compound $YMnO_3$ [24]. This difference is ascribed to the much larger tilt of the MnO_6 octahedra characteristic of quadruple perovskites.

All diffraction patterns in the whole 4–285 K range measured were refined in sequential mode in order to obtain the temperature dependence of the nuclear and magnetic structure. The temperature dependence of the moment (see Fig. 7) exhibits a typical mean-field behavior with no anomalies, which confirms the absence of additional long-range magnetic orderings of the A' sites. The refinement of the canted (M_y) component of the moment was carried out only below 80 K; at higher temperatures, this component becomes too small to be reliably refined.

B. Physical properties

1. *Specific heat*

Figure 8 shows the temperature behavior of the specific heat, C_p, measured at constant pressure. As expected from

TABLE III. B-site magnetic moment of $(YMn_3)Mn_4O_{12}$ in the $I2'/m'$ magnetic space group obtained from the structural refinement of the powder neutron diffraction data taken at 3.7 K (see Fig. 6).

	M_x	M_y	M_z	M	R_{Bragg}	R_{Mag}
Mn (B sites)	−2.2(1)	1.21(1)	2.4(1)	3.52(15)	8.86/6.13	3.52/5.10

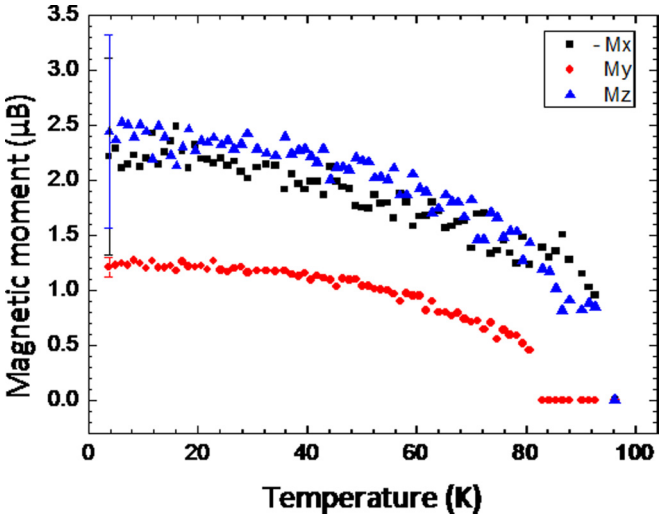

FIG. 7. Temperature dependence of the three components of the B-site moments obtained from the structural refinement of the powder neutron diffraction data. For clarity, error bars are indicated only at low temperature.

the previous structural analysis, the data show two pronounced jumps, $\Delta C_p^{T_S} \sim 65$ J mol^{-1} K^{-1} and $\Delta C_p^{T_{N,B}} \sim 22$ J mol^{-1} K^{-1}, at the structural and magnetic phase transitions, respectively. The jumps indicate that the two transitions are of second order, consistent with the behavior of the cell volume. The size of the jump at $T_S \sim 2 \times T_{N,B}$ is more than two times larger than the jump at $T_{N,B}$, which is attributed to the fact that the transition at T_S involves the lattice energy, while the transition at $T_{N,B}$ mainly involves the electronic energy. The absence of any further transition at low temperatures confirms the surprising finding of no long-range ordering of the A' ions. The C_p value at 300 K is 384 J mol^{-1} K^{-1} is to be compared

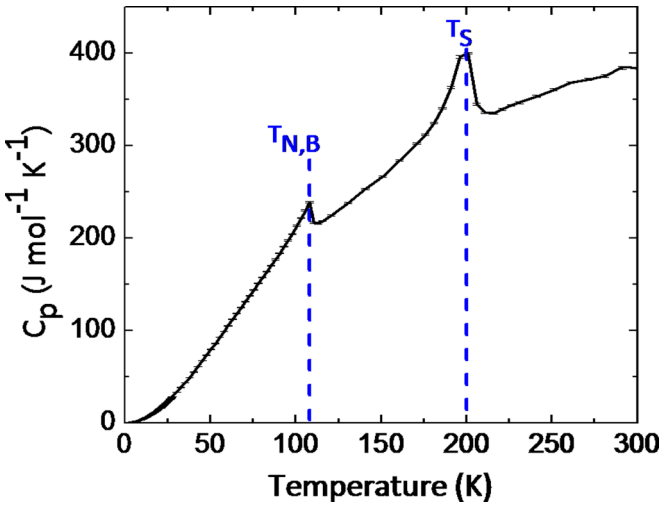

FIG. 8. Temperature dependence of the specific heat of $(YMn_3)Mn_4O_{12}$. Note the anomalies at the magnetic ordering of the B sites at $T_{N,B} = 108$ K and at the structural transition, $T_s = 200$ K, as discussed in Sec. III A.

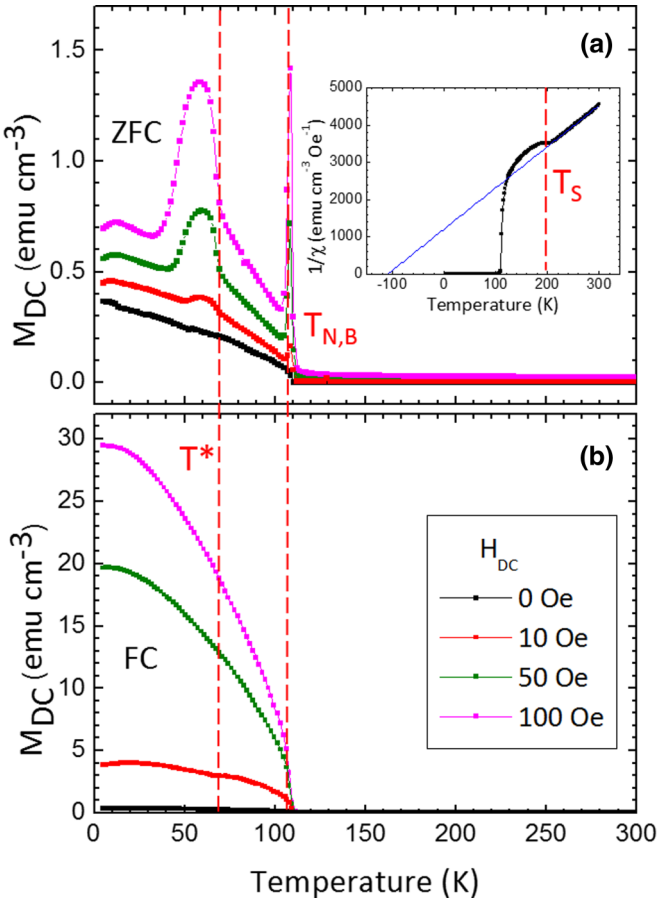

FIG. 9. (a) ZFC DC magnetization curves measured at 0, 50, and 100 Oe. Inset: Curie-Weiss fit of the inverse susceptibility in the paramagnetic 200–300 K region. (b) FC DC magnetization curves at 0, 50, and 100 Oe.

to the Dulong-Petit value of 498 J mol^{-1} K^{-1}, which suggests a Debye temperature larger than 300 K.

2. DC and AC magnetization

In Fig. 9, we plot the ZFC and FC DC magnetization curves, $M(T)$, measured at different fields of 0, 10, 50, and 100 Oe. The analysis of the paramagnetic region above $T_{N,B}$ highlights an anomaly of the $1/\chi$ curve at T_s, which indicates that the structural transition discussed above alters the superexchange interaction between Mn ions. Above this temperature, the $1/\chi$ curve displays a conventional Curie-Weiss behavior characterized by a Weiss constant $\Theta_W = -105 \pm 5$ K, which confirms the predominant AFM nature of Mn-O-Mn superexchange interaction. In the ZFC curves, a sharp field-dependent Hopkinson peak [25] at $T_{N,B}$ reflects a marked magnetic anisotropy, consistent with the C-type magnetic structure proposed. A fit of the Curie constant yields an effective moment of 5.02 μ_B, close to the value 4.9 μ_B expected for the high-spin state ($S = 2$) of Mn^{3+} ions by assuming a quenched orbital momentum. Below $T_{N,B}$, the ZFC and FC curves exhibit the characteristic behavior of a weak ferromagnet. This behavior, observed also in the ZFC curve measured at zero field (see black curve of Fig. 9), is quantitatively explained by a small difference of $\approx$0.004 μ_B

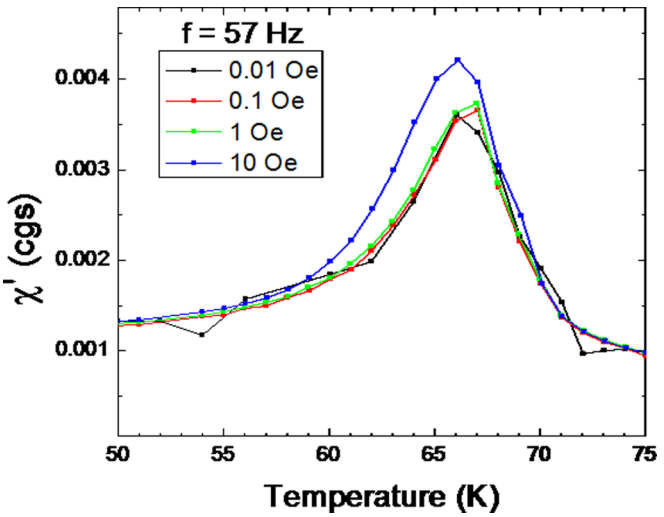

FIG. 10. Real part of the AC susceptibility measured at a frequency $f = 57$ Hz for different AC fields indicated in the legend. No significant changes are observed by changing either the field amplitude or f, as explained in the text.

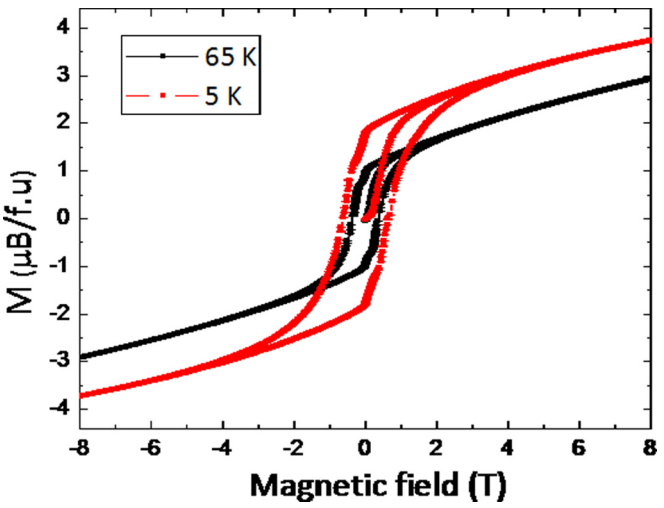

FIG. 11. Magnetization as a function of field up to 8 T at 5 and 65 K.

in the magnetic moments of the two $4e$ and $4f$ B sites, which is allowed by symmetry. This analysis justifies the above assumption of a tetragonal pseudosymmetry.

In the magnetic phase below $T_{N,B}$, the magnetization of the DC ZFC curves displays a broad peak in the at $T^* = 50$–70 K range. The intensity of this peak scales with the field and no peak is observed in the first magnetization curve taken after having completely suppressed the residual field of the magnet, as described in the experimental section. Under these conditions, the field is not larger than the earth magnetic field. The absence of any feature in the first magnetization curve below $T_{N,B}$ is coherent with the absence of additional magnetic peaks in the neutron diffraction data, which are also taken at zero field. The appearance of a broad peak in the ZFC data not observed in the first magnetization curve suggests a latent magnetic ordering at T^*.

In order to investigate the origin of this broad peak, we performed AC susceptibility measurements as a function of frequency f up to 10 kHz for field amplitudes in the 0.01–10 oersted range. Interestingly, a sharp peak is observed at the same temperature T_s where the dc data exhibit a broad peak for all amplitudes and for all frequencies. Neither the intensity nor the shape of the peak changes significantly either with field or with frequency up to 10 kHz. Figure 10 shows representative curves of the real part χ' for different fields taken at $f = 57$ Hz. Further work is needed to elucidate the origin of this magnetic response, which supports the picture of latent magnetic ordering.

Figure 11 shows the dependence of the magnetization as a function of field up to 8 T measured at 5 and 65 K. At both temperatures, the linear behavior observed at high field and the existence of a sizable hysteresis support the picture of weak FM. Interestingly, the coercive field is significantly larger than in other $(A\mathrm{Mn_3})\mathrm{Mn_4O_{12}}$ compounds [4,11,26–28], which is attributed to a stronger magnetic anisotropy.

IV. CONCLUSION

In conclusion, we have reported on the successful high pressure synthesis of the single valent Mn^{3+} $(\mathrm{YMn_3})\mathrm{Mn_4O_{12}}$ quadruple perovskite, where the insertion of the small Y^{3+} ion in the A site exerts a significant chemical pressure, which is expected to enhance the strength of the superexchange interaction between neighboring Mn^{3+} ions. A systematic study of the structural and physical properties confirms this expectation; we have found a significant 30 K enhancement of the AFM ordering temperature of the Mn^{3+} B sites with respect to the case of the isostructural and isovalent compound $(\mathrm{LaMn_3})\mathrm{Mn_4O_{12}}$ reported previously. We argue that this enhancement is promising in view of future developments of quadruple perovskites as magnetic ferroelectrics. On the other hand, we have surprisingly found no long-range ordering of the Mn^{3+} A' sites; instead, a broad peak of the dc magnetization at $T^* = 50$–70 that disappears in the first magnetization ZFC curve and a sharp peak of the ac susceptibility at the same temperature suggests a latent order of these sites. A further unexpected feature of $(\mathrm{YMn_3})\mathrm{Mn_4O_{12}}$ is the occurrence of a structural second-order phase transition at $T_s = 200$ K, which is concomitant to an anomalous behavior of the unit cell and of most Mn-O bonds. A BVS analysis suggests that this transition is associated with a partial charge redistribution involving both A' and B Mn sites, which may alter the AFM interaction between neighboring Mn ions. Further experiments are needed to explain the absence of long-range ordering of the A' sites and to investigate the origin of the structural transition at T_s and the possibility of magnetic ferroelectricity.

ACKNOWLEDGMENTS

The authors are grateful to F. Bolzoni, R. Cabassi, G. Calestani, D. Hrabovsky, and M.-B. Lepetit for stimulating discussions, T. Roisnel, L.-M. Chamoreau, D. Frost, and

H. Keppler for their invaluable assistance in the structural refinement, in the single-crystal diffraction measurements and in the high-pressure synthesis. The authors gratefully acknowledge the support of the German Science Foundation for synthesis at the Bayerisches Geoinstitut, and the Laue-Langevin Institut. M.V. gratefully acknowledges financial support from the "Leonardo da Vinci" doctoral program of the Franco-Italian university.

[1] M. Marezio, P. D. Dernier, J. Chenavas, and J. C. Joubert, J. Solid State Chem. **6**, 16 (1973).
[2] A. Deschanvres, B. Raveau, and F. Tollemer, Bull. Soc. Chim. Fr. **11**, 4077 (1967).
[3] A. Prodi, E. Gilioli, A. Gauzzi, F. Licci, M. Marezio, F. Bolzoni, Q. Huang, A. Santoro, and J. W. Lynn, Nat. Mater. **3**, 48 (2004).
[4] G. Zhang, S. Dong, Z. Yan, Y. Guo, Q. Zhang, S. Yunoki, E. Dagotto, and J.-M. Liu, Phys. Rev. B **84**, 174413 (2011).
[5] R. D. Johnson, L. C. Chapon, D. D. Khalyavin, P. Manuel, P. G. Radaelli, and C. Martin, Phys. Rev. Lett. **108**, 067201 (2012).
[6] X. Z. Lu, M.-H. Whangbo, S. Dong, X. G. Gong, and H. J. Xiang, Phys. Rev. Lett. **108**, 187204 (2012).
[7] R. Shannon, Acta. Cryst. **A32**, 751 (1976).
[8] B. Bochu, J. Chenavas, J. C. Joubert, and M. Marezio, J. Solid State Chem. **11**, 88 (1974).
[9] F. Mezzadri, G. Calestani, M. Calicchio, E. Gilioli, F. Bolzoni, R. Cabassi, M. Marezio, and A. Migliori, Phys. Rev. B **79**, 100106(R) (2009).
[10] F. Mezzadri, M. Calicchio, E. Gilioli, R. Cabassi, F. Bolzoni, G. Calestani, and F. Bissoli, Phys. Rev. B **79**, 014420 (2009).
[11] A. Prodi, E. Gilioli, R. Cabassi, F. Bolzoni, F. Licci, Q. Huang, J. W. Lynn, M. Affronte, A. Gauzzi, and M. Marezio, Phys. Rev. B **79**, 085105 (2009).
[12] E. Gilioli, G. Calestani, F. Licci, C. Paorici, A. Gauzzi, F. Bolzoni, and A. Prodi, J. Solid State Chem. **179**, 3839 (2006).
[13] R. Clark and J. Reid, Acta Crystallogr. A **51**, 887 (1995).
[14] Agilent (2014). CrysAlis PRO. Agilent technologies Ltd, Yarnton, Oxfordshire, England.
[15] O. Dolomanov, L. Bourhis, R. Gildea, J. Howard, and H. Puschmann, Appl. Crystallogr. **42**, 339 (2009).
[16] G. Sheldrick, Acta Crystallogr. A **71**, 3 (2015).
[17] J. Rodriguez-Carvajal, Physica B **192**, 55 (1993).
[18] See Supplemental Material at http://link.aps.org/supplemental/10.1103/PhysRevMaterials.1.064407 for tables refinement of $(YMn_3)Mn_4O_{12}$ single crystal x-ray diffraction data obtained at room temperature.
[19] K. Gautam, D. K. Shukla, S. Francoual, J. Bednarcik, J. R. L. Mardegan, H.-P. Liermann, R. Sankar, F. C. Chou, D. M. Phase, and J. Strempfer, Phys. Rev. B **95**, 144112 (2017).
[20] B. Bochu, J. Buevoz, J. Chenavas, A. Collomb, J. Joubert, and M. Marezio, Solid State Commun. **36**, 133 (1980).
[21] H. Etani, I. Yamada, K. Ohgushi, N. Hayashi, Y. Kusano, M. Mizumaki, J. Kim, N. Tsuji, R. Takahashi, N. Nishiyama, T. Inoue, T. Irifune, and M. Takano, J. Am. Chem. Soc. **135**, 6100 (2013).
[22] J. B. Goodenough, Phys. Rev. **100**, 564 (1955).
[23] T. Moriya, Phys. Rev. **120**, 91 (1960).
[24] I. V. Solovyev, M. V. Valentyuk, and V. V. Mazurenko, Phys. Rev. B **86**, 054407 (2012).
[25] J. Hopkinson, Philos. Trans. R. Soc. London A **180**, 443 (1889).
[26] T. Locherer, R. Dinnebier, R. Kremer, M. Greenblatt, and M. Jansen, J. Solid State Chem. **190**, 277 (2012).
[27] Y. S. Glazkova, N. Terada, Y. Matsushita, Y. Katsuya, M. Tanaka, A. V. Sobolev, I. A. Presniakov, and A. A. Belik, Inorg. Chem. **54**, 9081 (2015).
[28] D. Delmonte, F. Mezzadri, C. Pernechele, G. Calestani, G. Spina, M. Lantieri, M. Solzi, R. Cabassi, F. Bolzoni, A. Migliori, C. Ritter, and E. Gilioli, Phys. Rev. B **88**, 014431 (2013).